Numerical and Experimental Investigation of a Brushless Motor Test Bench Equipped with a X5C-02 Propeller

Saoussane Gouiaa, Ameni Mehdi, Zied Driss[*], Bilel Ben Amira, Mohamed Salah Abid

Laboratory of Electro-Mechanic Systems (LASEM), National School of Engineers of Sfax (ENIS), University of Sfax (US),
B.P. 1173, Road Soukra km 3.5, 3038 Sfax, TUNISIA
*Corresponding author: zied.driss@enis.tn

Abstract In this paper, a computer simulation has been done to study the aerodynamic structure around a X5C-02 main blades propeller. The numerical model is based on the resolution of the Navier-Stokes equations with a standard k-ε model. The local characteristics are determined using the software "Solidworks Flow Simulation". The software gives us the opportunity to extract the global result of this system which is the force of the thrust. The validation of this result has been done using an experimental protocol designed in the laboratory named brushless motor test bench. In this paper, we have described the experimental set up and we have compared it with the numerical curve using two meshes.

Keywords: *computer simulation, X5C-02 propeller, aerodynamic structure, validation with experiments, brushless motor test bench*

1. Introduction

The study of the aerodynamic structure around a propeller has a big importance especially at the laboratory scale. This type of rotors is used in the UAVs which can be utilized in the civil as well as the military applications. Eisenbei [1] said that these types of multi-copters are used especially in case of risk situations. In this context, it will be interesting to solve the problems related to the propellers. Due to their low performances, the academic researchers tend to make new designs of main blades and effectuate many experiments. These experimental protocols are used to ameliorate the efficiency of the propellers. The validation of the results has been done via comparison of experiments and computational results deduced from the CFD. For example, Shi et al. [2] used the CFD simulation to predict unsteady aerodynamic flow around helicopter rotors in hover and forward flight around a single-blade. Also, Ansari et al. [3] reviewed the main approaches found in the literature, categorized them into steady-state, quasi-steady, semi empirical and fully unsteady methods used in the aerodynamic modeling of insect-like flapping flight for micro air vehicles. Cetinsoy et al. [4] presented a method for studying and designing of a new unmanned aerial vehicle. In this paper, many experiments have been done to enhance the operational performance of the UAV especially aerodynamic and mechanical designs optimization. Song et al. [5] studied the problem of flapping motion control of Micro Air Vehicles. In fact, based on the knowledge of the hummingbird, a dynamic model was developed. They proposed to control the performance by learning from experience and validate the results with numerical simulations. The paper of Jinoh et al. [6] presented an experimental study on time delay control of actuation system of tilt rotor unmanned aerial vehicle. In fact, the actuation system should be controlled to track the position sent from the flight controller. The experimental results show that the following control performance specifications are satisfied under load. Jinoh et al. [6] studied the performance of the UAV especially its control system. Strawn et al. [7] showed some highlights from CFD modeling and development of rotorcrafts. The paper mentioned many references that used the validation between the computational simulations and experiments. Caradonna et al. [8] presented the experimental and analytical studies of a model helicopter rotor in hover. From the mentioned studies, it appears interesting to make many computational simulations and compare them with the investigated experiments using different type of propellers which leads to ameliorate the performance of the whole UAV. In this paper, we are interested on the study of an X5C-02 main blades propeller. To validate our numerical model, we have compared the numerical results with our experiments data.

2. Geometrical Arrangement

Figure 1 presents the geometrical model composed of a motor with a cylindrical form, the propeller mounted on it and a spinner that cover the motor. Figure 2 illustrates the different dimensions of the propeller.
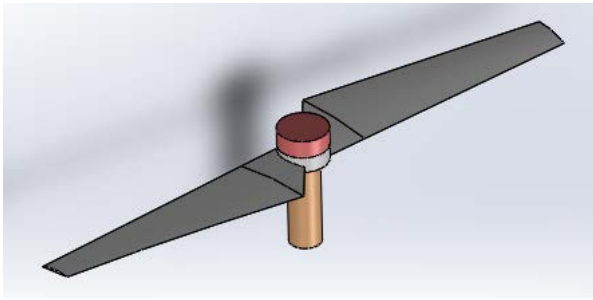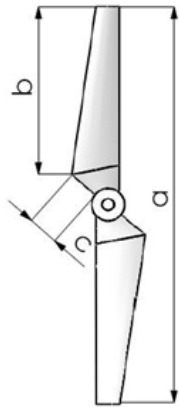
Figure 1. 3D presentation of the geometrical model

Dimensions	Values (mm)
a	135
b	55
c	10

Figure 2. Dimensions of the propeller

3. Numerical Model

To study the flow around the X5C-02 propeller, the computational fluid dynamic CFD simulations are used. These simulations are included in the CFD code of the software Solidworks Flow Simulation [9]. The used code is based on the resolution of the Navier-Stokes equations [10,11]. The k-ε turbulence model was used to analyze the turbulent flow [12,13]. A necessary step to simulate the model is the determination of the boundary conditions. In this application, the value of the pressure is 101325 Pa and the air molecular mass is equal to 0.02896 kg/mol.

4. Numerical Results

In this part, we present the local characteristics in the different planes defined by x=0 mm, y=0 mm and z=0 mm. Particularly, we are interested on the distribution of the average velocity, the static pressure, the turbulent kinetic energy, the dissipation rate of the turbulent kinetic energy and the turbulent viscosity.
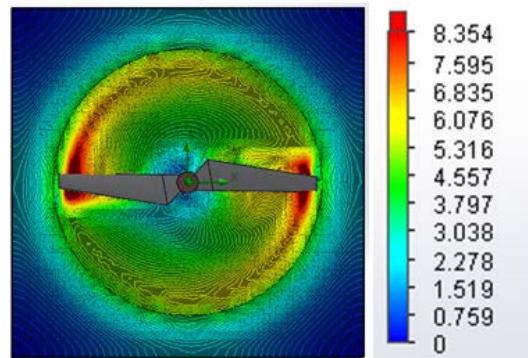
4.1. Average Velocity

Figure 3 presents the distribution of the average velocity in the visualization planes defined by x=0 mm, y=0 mm and z=0 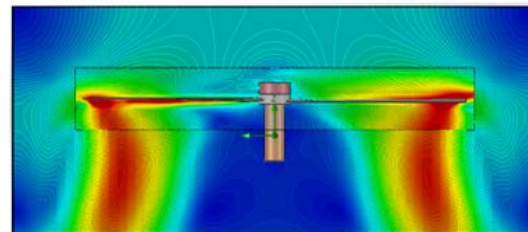mm. According to the different selected views, it has been noted that the high values of the average velocity are concentrated in the propeller especially on its bottom. Near the motor, the linear velocity has low values. In the outer of the rotary volume, the same phenomenon has been noted.
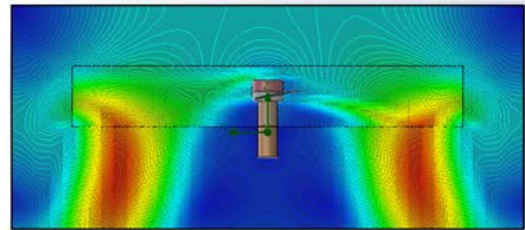

Figure 3. Distribution of the average velocity
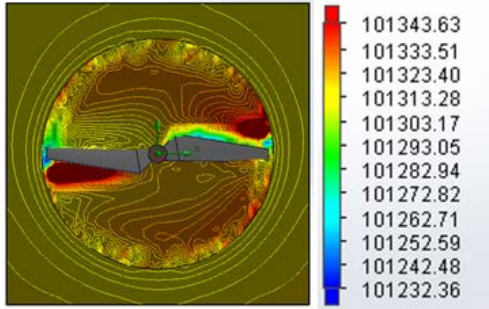
4.2. Static Pressure

Figure 4 shows the distribution of the static pressure in the visualization planes defined by x=0 mm, y=0 mm and z=0 mm. According to these results, it has been noted that the top of the propeller is characterized by a depression zone characterized by low values of the static pressure contrarily to its bottom characterized by a depression zone characteristic by the highest values. Indeed, it has been noted that the two blades of the propeller do not have the same static pressure distribution due to the propeller inclination.
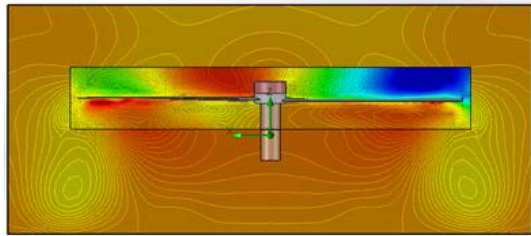
4.3. Turbulent Kinetic Energy

Figure 5 illustrates the distribution of the turbulent kinetic energy in the different presentation planes. According to these results, it has been observed that the turbulent kinetic energy is low in the whole volume except in the extremities of the propeller. In this zone, a wake characteristic of the maximum value of the turbulent kinetic energy has been observed. In these conditions, the maximum value of the turbulent kinetic energy is equal to k = 1.49 J/kg.
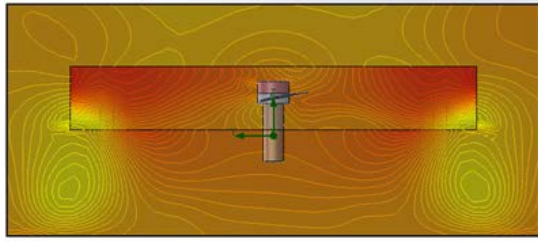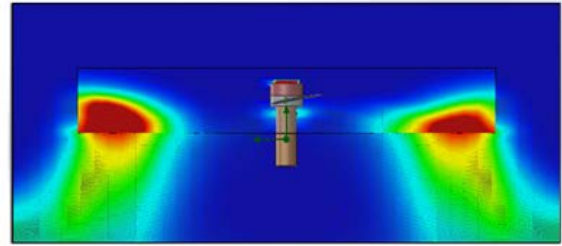
(a) Plane x=0 mm

(b) Plane z=0 mm

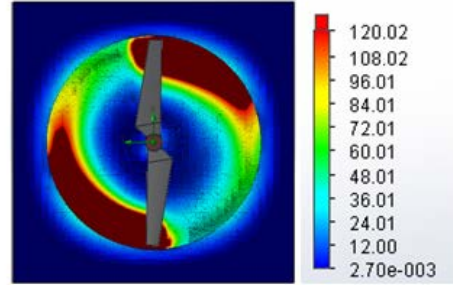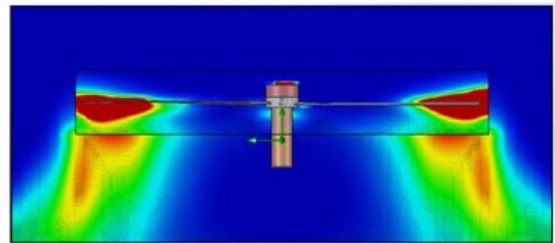(c) Plane y = 0 mm

Figure 4. Distribution of the static pressure
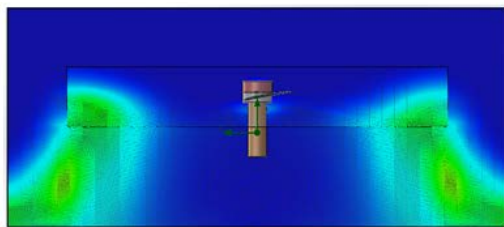

(a) Plane x=0 mm
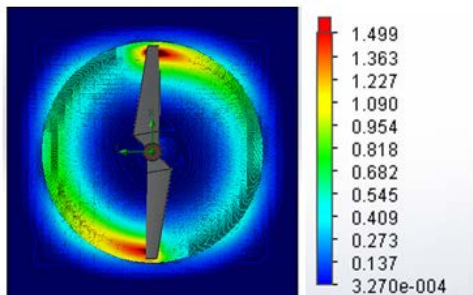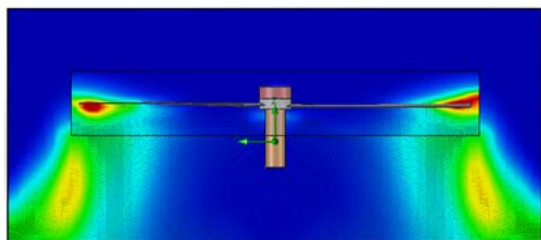

(b) Plane z=0 mm

(c) Plane y=0 mm

Figure 6. Distribution of the dissipation rate of the turbulent kinetic energy

(a) Plane x = 0 mm

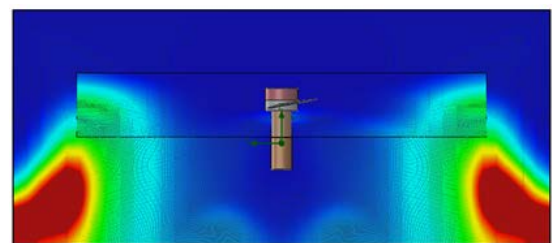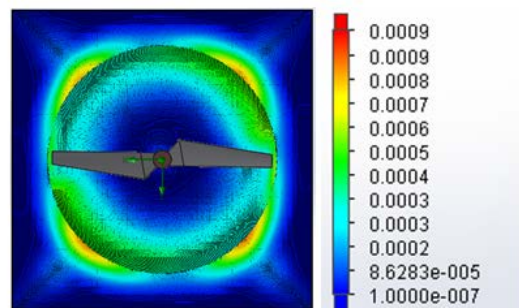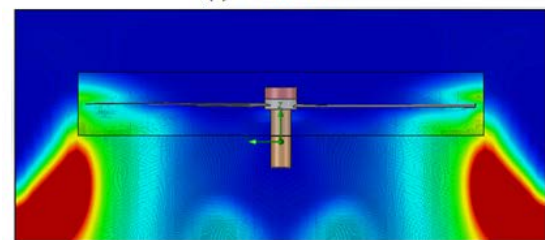

(b) Plane z = 0 mm

(c) Plane y = 0 mm

Figure 5. Distribution of the turbulent kinetic energy

(a) Plane x=0 mm

(b) Plane z=0 mm

(c) Plane y=0 mm

Figure 7. Distribution of the turbulent viscosity

4.4. Dissipation Rate of the Turbulent Kinetic Energy

Figure 6 shows the variation of the dissipation rate of the turbulent kinetic energy in the different chosen planes. According to these results, it has been noted that the two extremities of the propeller present a high value of the dissipation rate of the turbulent kinetic energy. This distribution is the same founded with the turbulent kinetic energy. This fact is explained since the propeller which is the element having the maximum values of the turbulent kinetic energy should be the one which dissipates the maximum values.

4.5. Turbulent Viscosity

Figure 7 presents the distribution of the turbulent viscosity in the visualization planes. In each planes, it has been noted that the turbulent viscosity presents a low value in the whole volume. In the end of the rotating volume, the turbulent viscosity becomes important compared to the other parts of the system. In these conditions, the maximum value of the turbulent viscosity is equal to $\mu t = 9.10\text{-}3$ Pa.s.

5. Measure of the Thrust Force

The thrust is expressed according to the number of revolutions. Using an experimental approach, we carry out a slotted measuring section which functions according to the following kinematic diagram shown in Figure 8 (a). It illustrates the connectivity of links and joints of the mechanism rather than the dimensions or shape of the parts and gives a simplified representation allowing a better comprehension of operation. This bench is composed of a propeller mounted in a brushless motor. This assembly is the system that we will measure its thrust when rotating. It is also composed of a beam having the role of a support for the test. The final component of this test bench is the digital scale which will measure the value of the thrust in the form of a mass. The aim of the brushless motor test stand is to evaluate the motor and rotor characteristics. In fact, one of the challenges of rotor testing is the measurement of the thrust created when it is mounted in the motor. In order to design a brushless motor test stand, it is very necessary to know the law that we should use. In fact, the thrust produced by the rotor when it is mounted in the motor can be measured by the digital scale in the form of a mass. According to the following schematic presentation of the brushless motor test stand shown in Figure 8 (b), this bench has the form of an isosceles triangle ABC. So, to satisfy the condition of the thrust, the distance AB should be equal to AC and the angles $\widehat{ABC}$ and $\widehat{ACB}$ should be equal to 45°.

5.1. Experimental Set Up

After preparing all the needed components and wiring the receiver circuit, it is necessary to do many instructions in order to realize the experience. In fact, we should follow the next steps:
- Charge the Lipo battery

- Make the batteries of the remote control in the right place
- Adjust the zero of the digital scale
- Calibrate the numerical speed sensor at the unit "rpm"
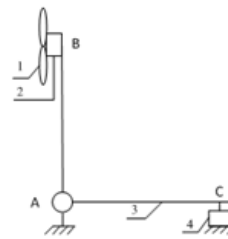
N°	Designation
4	Digital scale
3	Beam
2	Brushless motor
1	Propeller

(a) Kinematic schema of the brushless motor test stand
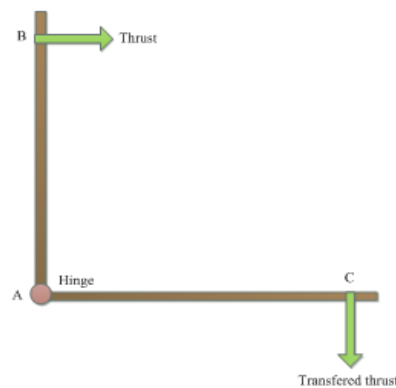
(b) Schematic presentation of the brushless motor test stand

Figure 8. Schematization of the theoretical principle of the test bench

(a) Thrust laboratory test

(b) Principle operation of the tachometer

Figure 9. Thrust laboratory test and principle operation of the tachometer

Besides, we should fix the utilized components in right places like shown in Figure 9 (a). The principal of this

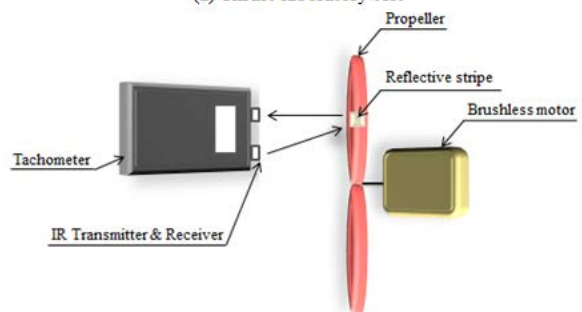experiment is very simple. The whole objective is to measure the value of thrust in g corresponding to each value of rotational speed. To do this, we tried firstly to vary the speed with the remote control. Then, we read its value via the tachometer. It is a digital speed sensor which uses the principle of reflection of the light. It is equipped with a LED which emits a light which will be reflected on a reflective like shown in the Figure 9 (b) and returns towards the aircraft equipped with a receiver. Speed is measured including the frequency to which the beam is considered. Finally, we extract the value of the thrust written in the screen of the digital scale. Due to some errors coming from the measurement instruments and the errors of reading, we have repeated the experiment more than one time in order to get the most correct values. This will help us to plot the most adequate curve force of thrust in function of the rotation speed.

5.2. Plotting the Curve

After measuring the thrust in grams at different values of rotational speed, we have converted these values into N via multiplying them by the gravitational acceleration g. The variation of the force F (N) in function of the rotating speed Ω (rpm) can be plotted as represented in Figure 10. According to these results, it is clear that the value increases, with the increase of the rotation speed. In these conditions, the maximum value of the thrust is equal to F=0.215 N for a rotating speed equal to Ω=8307 rpm. The variation of the curve force in function of the number of revolutions presents a not linear evolution of the force according to the rotational speed. Also, we can deduce that the increase of the value of the rotational speed generates the increase of the value of the created thrust.
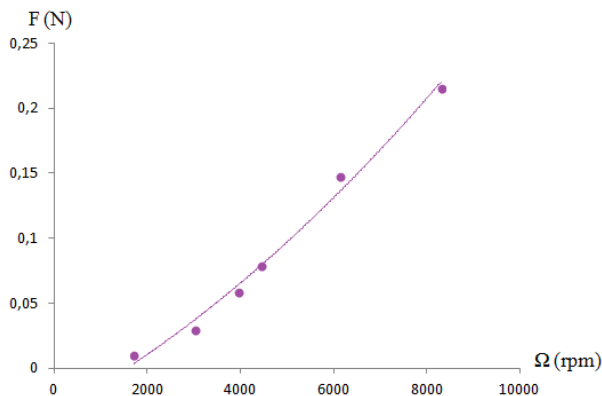

Figure 10. Variation of the thrust F(N) in function of the rotating speed Ω (rpm)

6. Comparison with Experimental Results

In our study, the force is considered as a global result. In fact, after doing the experience and plotting the corresponding curve, we have to determine the numerical force produced at every rotational speed and plot the curve. The curves presenting the variation of the force in function of the rotation speed is shown in Figure 11 for two types of mesh. The first mesh is an automatic type with N=11756 and the second is a manual type with

N=139417. These two curves are drawn in the same referential with the experimental results in order to be compared. According to these results, it is clear that the curve of the numerical force with a manual mesh and the experimental one are approximately superposed. This means that the chosen mesh is the optimal one.
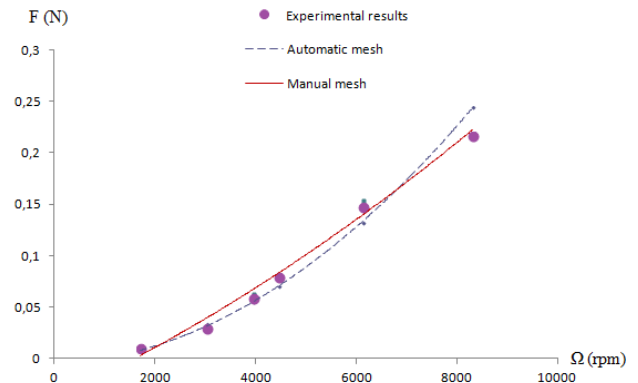

Figure 11. Variation of the force in function of the rotational speed

7. Conclusion

Computer simulations have been developed to study the aerodynamic structure around a X5C-02 main blades propeller. It has been noted that the dimensions of the propeller has a direct effect on the local characteristics of the aerodynamic structure. Particularly, it has been noted that the depression zones are located especially on the top of the propeller. Also, the wake zones are located at the extremities of the propeller and the rotating volume. The value of the thrust force increases with the value of the rotating speed. The comparison of the numerical results with the experiment done using our brushless motor test bench shows a good agreement, especially using a manual mesh.

In further works, it will be important to determine the local characteristics and extract the thrust force around a multi-copter with many propellers to define the zone of consumption of energy and how to ameliorate its performance.

References

[1] H. Eisenbei, *UAV photogrammetry*, University of Technology Dresden, 2009.

[2] Y. Shi, Q. Zhao, F. Fan, G. Xu, *A new single-blade hybrid CFD method for hovering and forward-flight rotor computation*, Chinese Journal of Aeronautics 24(2011) 127-135.

[3] S. Ansari, R Zbikwoski., K. Knowles, *Aerodynamic modeling of insect-like flapping flight for micro air vehicles*,Progress in Aerospace Sciences 42(2006), 129-172.

[4] E. Cetinsoy, S. Dikyar, C. Hancer, K.T. Oner, E. Sirimoglu, M. Unel, M.F. Aksit, *Design and construction of a novel quad-tilt wing UAV*, Mechatronics 22(2012), 732-745.

[5] Y.D. Song, L. Weng, G. Lebby, *Human memory/learning inspired control method for flapping-wing micro air vehicles*, Journal of Bionic Engineering 7(2010), 127-133.

[6] L. Jinoh, Y. Changsun, Y. Park, B. Park, S. Lee, D.G. Gweon, P.Y. Chang, *An experimental study on time delay control of actuation system of tilt rotor unmanned aerial vehicle*, Mechatronics 22(2012), 184-194.

[7] R.C. Strawn, F.X. Caradonna, E.P.N Duque, *30 years of rotorcraft computational Fluid Dynamics research and development*, Journal of the American Helicopter Society, 2005.

[8] F.X. Caradonna, C. Tung, *Experimental and analytical studies of a model helicopter rotor in hover*, Vertica, Vol. 5, (2), 1981, pp. 149-161.

[9] Z. Driss, O. Mlayah, S. Driss, D. Driss, M. Maaloul, M.S. Abid, Study of the bucket design effect on the turbulent flow around unconventional Savonius wind rotors, Energy, pp. 708-729, Vol. 89, 2015.

[10] S. Driss, Z. Driss, I. Kallel Kammoun, Computational study and experimental validation of the heat ventilation in a living room with a solar patio system, Energy & Buildings, pp. 28-40, Vol. 119, 2016.

[11] A. Bouabidi, Z. Driss, N. Cherif, M.S. Abid, Computational investigation of the external excitation frequency effect on liquid sloshing phenomenon, WSEAS Transactions on Fluid Mechanics, pp. 1-9, Volume 11, 2016.

[12] S. Frikha, Z. Driss, H. Kchaou, M.S. Abid, *Incidence angle effect on the turbulent flow around a Savonious wind rotor*, American Journal of Energy Research, 2016, Vol. 4, No. 2, 42-53.

[13] S. Hadj Kacem , M.A. Jemni, Z. Driss, M.S. Abid, *The effect of H2 enrichment on in-cylinder flow behavior, engine performances and exhaust emissions: Case of LPG hydrogen engine*, Applied Energy 179(2016), 961-971.